Circulation Journal
Official Journal of the Japanese Circulation Society
http://www.j-circ.or.jp

ORIGINAL ARTICLE
Imaging

Combined Supine and Prone Myocardial Perfusion Single-Photon Emission Computed Tomography With a Cadmium Zinc Telluride Camera for Detection of Coronary Artery Disease

Yoshiko Nishiyama, MD; Masao Miyagawa, MD, PhD; Naoto Kawaguchi, MD; Masashi Nakamura, MD; Tomoyuki Kido, MD, PhD; Akira Kurata, MD, PhD; Teruhito Kido, MD, PhD; Akiyoshi Ogimoto, MD, PhD; Jitsuo Higaki, MD, PhD; Teruhito Mochizuki, MD PhD

Background: Myocardial perfusion SPECT (MPS) traditionally requires the patient to be in the supine position, but diaphragmatic attenuation of the inferior wall reduces test specificity. The aim of this study was to assess the feasibility of combined MPS in the supine and prone positions using a novel cadmium zinc telluride (CZT) camera.

Methods and Results: A total of 276 consecutive patients with suspected/known coronary artery disease (CAD) who underwent single-day ^{99m}Tc-tetrofosmin or ^{99m}Tc-sestamibi stress/rest CZT SPECT, were enrolled in the study. Seventy-six underwent coronary angiography. Five-minute scan in the supine (S) position and thereafter in the prone (P) position produced images that were visually interpreted to obtain summed stress (SSS) and rest (SRS) scores. A combined stress score (C-SSS) was calculated by grouping anterior perfusion defects observed during supine imaging with inferior half segments observed during prone imaging. The SSS for the supine, prone, and combined protocols were 9±8, 7±8, and 7±8, respectively (P<0.0001). The SRS were 5±8, 4±7, and 6±7, respectively (P=0.005). The area under the ROC curve for the S-SSS, P-SSS, and C-SSS scores was 0.815 (95% CI: 0.713–0.917), 0.813 (0.711–0.914), and 0.872 (0.783–0.961), respectively. Corresponding sensitivities and specificities for detecting CAD were 87% and 50%, 80% and 77%, and 85% and 82%, respectively. C-SSS had significantly better specificity and accuracy than S-SSS (P<0.05).

Conclusions: Combined imaging with a CZT camera is suitable for routine clinical MPS and provides greater diagnostic accuracy than supine imaging alone. (*Circ J* 2014; **78:** 1169–1175)

Key Words: Cadmium zinc telluride; Coronary artery disease; Myocardial ischemia; Prone imaging; Single-photon emission computed tomography

Myocardial perfusion single-photon emission computed tomography (MPS) is the most common non-invasive imaging technique for risk assessment and treatment selection among patients with coronary artery disease (CAD). It has traditionally been performed with patients in the supine position, but the resulting images often include diaphragmatic attenuation of the inferior wall, causing false-positive inferior wall defects that reduce test specificity. Segall et al initially described MPS with data acquisition in the prone position.[1,2] Subsequently, several studies with ^{201}Tl or ^{99m}Tc-sestamibi MPS showed that imaging acquisition in the prone position improved the specificity for evaluating inferior wall abnormalities by minimizing diaphragmatic attenuation.[3–6] These studies, however, used conventional Anger cameras, which have significant technological limitations, including a greater period required for image acquisition, and complicated protocols.

Recently, a novel ultrafast gamma camera – the Discovery NM530c (GE Healthcare, Haifa, Israel) – has been developed. This camera is based on a multi-pinhole design and has cadmium zinc telluride (CZT) solid-state detectors.[7] The CZT camera has greater photon sensitivity and spatial resolution than the conventional Anger camera.[8–12] In consequence, it can reduce the MPS acquisition time by up to one-fifth.[13] Shorter image acquisition times may be suitable for combined supine and prone imaging, but no comprehensive study has focused only on com-

Received October 25, 2013; revised manuscript received December 25, 2013; accepted January 7, 2014; released online February 25, 2014
Time for primary review: 11 days
Department of Radiology (Y.N., M.M., N.K., M.N., Tomoyuki K., A.K., Teruhito K., T.M.), Department of Integrated Medicine and Informatics (A.O., J.H.), Ehime University Graduate School of Medicine, Toon, Japan
Mailing address: Yoshiko Nishiyama, MD, Department of Radiology, Ehime University Graduate School of Medicine, Shitsukawa, Toon 791-0295, Japan. E-mail: yo527@m.ehime-u.ac.jp
ISSN-1346-9843 doi:10.1253/circj.CJ-13-1316

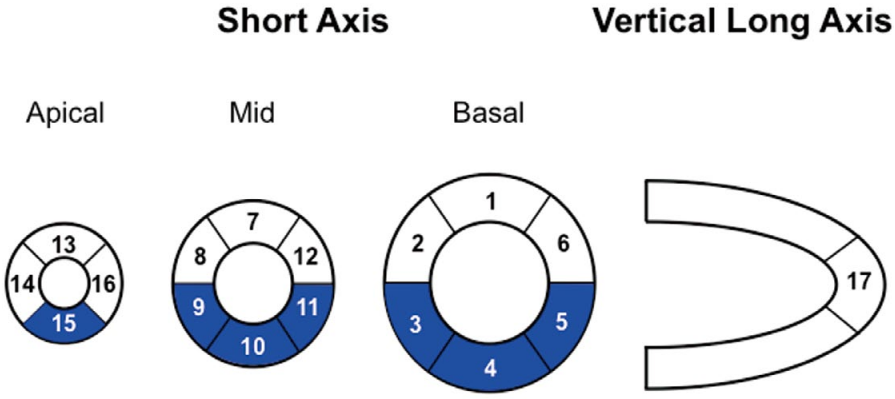

Figure 1. Assignment of myocardial regions in a 17-segment model for the interpretation of single-photon emission computed tomography (SPECT) images. A combined stress score was calculated by grouping the anterior defects observed during supine imaging (white) with inferior half segments (blue) observed during prone imaging. The inferior half segments correspond to segments 3–5, 9–11, and 15. To match the results with coronary angiograms, segments 3, 4, 9, 10, and 15 were grouped into the right coronary artery territory, segments 5, 6, 11, 12, and 16 into the left circumflex artery territory and all other segments into the left anterior descending artery territory.

paring these imaging positions. Therefore, the aim of this study was to assess the feasibility of CZT single-photon emission computed tomography (SPECT) performed in both the supine and prone positions and to compare the diagnostic accuracy with that of invasive coronary angiography (CAG).

Methods

Patients

We enrolled 276 consecutive patients with suspected or known stable CAD who were referred for pharmacological stress/rest MPS. All patients underwent single-day ^{99m}Tc-tetrofosmin or ^{99m}Tc-sestamibi stress/rest MPS with a CZT camera. A total of 270 patients underwent CZT SPECT in both the supine and prone positions; imaging in the prone position was not possible for 6 patients who had a chest tube or some form of palsy, and these patients were hence excluded from the study. A subgroup of 76 patients (46 men and 30 women) underwent invasive CAG for clinical reasons within 3 months of MPS. None experienced a myocardial infarction or required revascularization in the interval between the MPS and CAG. The exclusion criteria for the present study were as follows: (1) acute myocardial infarction; (2) unstable angina; (3) history of previous coronary artery bypass grafting; (4) myocardial revascularization 60 days before MPS; (5) atrioventricular block greater than the first degree; (6) non-ischemic cardiomyopathy; (7) known history of bronchial asthma; and (8) valvular heart diseases. The study was approved by the Ethics Committee of Ehime University (No. 1212003), and all patients provided informed consent.

Study Protocol

The patients underwent stress/rest electrocardiogram (ECG)-gated CZT SPECT with a single-day protocol. They were instructed to refrain from consuming beverages containing caffeine for at least 24 h before the test. ^{99m}Tc-tetrofosmin (n=179) or ^{99m}Tc-sestamibi (n=97) stress/rest SPECT was performed in both the supine and prone positions using a CZT camera (Discovery NM 530c; GE Healthcare). Pharmacological stress was induced with adenosine triphosphate disodium (ATP) infused at a rate of 160 $\mu g \cdot kg^{-1} \cdot min^{-1}$ over 5 min.[14,15] After 3 min of ATP infusion, ^{99m}Tc-tetrofosmin (n=175) or ^{99m}Tc-sestamibi (n=95) was injected at a dose ranging from 296 to 370 MBq and imaging was started 60 min later. Five-minute data acquisition was performed first in the supine position and immediately thereafter in the prone position using the CZT gamma camera. Four hours later, resting CZT SPECT was performed via an identical acquisition protocol 90 min after the injection of 740 MBq ^{99m}Tc myocardial perfusion agents. Images were reoriented into short-axis and vertical and horizontal long-axis slices and were also displayed in a polar plot format using standard software (QPS, Los Angeles, CA, USA).[16] The estimated total radiation exposure with this protocol was 4.86–9.58 mSv. The effective dose was determined based on data in ICRP publications 80 and 106.[17,18]

Acquisition and Reconstruction of CZT SPECT

The CZT camera is equipped with a multiple-pinhole collimator and 19 stationary CZT detectors, simultaneously imaging 19 cardiac views. Each detector contains 32×32 pixilated 5-mm-thick (2.46×2.46 mm) elements. System design enables imaging of a 3-D volume imaged simultaneously by all detectors. Patients were imaged in the supine position with arms placed over the head. List files were acquired and stored.

All SPECT images were reconstructed on a standard workstation (Xeleris Ver. 3.0; GE Healthcare) using a commercially available dedicated software package (Myovation for Alcyone; GE Healthcare) with an iterative algorithm based on integrated collimator geometry modeling, using maximum likelihood iterative reconstruction to obtain perfusion images in standard axes as previously reported.[8] In brief, 40 and 50 iterations of the algorithm were used for reconstruction of the stress and rest datasets, respectively. A Butterworth post-processing filter was applied (cut-off frequency, 0.37 cycle/cm; order, 7) to the reconstructed slices. Images were reconstructed without attenuation correction.

Image Quality Analysis

A quality assessment of both the stress and rest SPECT im-

ages was performed by visually grading each image using a 4-point scale, as follows: 1, poor; 2, fair; 3, good; or 4, excellent. Visualization, myocardial count density and uniformity, and endocardial and epicardial edge definitions were considered. Moreover, the degree of extra-cardiac radioactivity was assessed using a 3-point scale: 1, no extra-cardiac activity in the field of view or minor activity not adjacent to the myocardium; 2, minor extra-cardiac activity adjacent to the myocardium; and 3, moderate–severe extra-cardiac activity interfering with interpretation. Two experienced nuclear cardiology physicians who were blinded to the coronary anatomy and clinical results independently performed the qualitative analysis. Their scores for image quality and extra-cardiac activity were compared and if any difference was noted the worse score (lower score for quality and higher score for extra-cardiac activity) was applied.

Image Interpretation and Quantitative Analysis

The stress and rest perfusion CZT SPECT images were also semi-quantitatively scored using a 17-segment model[19] of the left ventricle (LV) and a 5-point scale (0, normal; 1, mildly reduced; 2, moderately reduced; 3, severely reduced; and 4, absent). The summed stress score (SSS) and summed rest score (SRS) were calculated by adding the scores for the 17 segments in the stress and rest images, respectively. In addition, a combined stress score was calculated by grouping anterior defects observed during supine imaging with inferior half segments observed during prone imaging (**Figure 1**). SSS <4 was considered normal; a score between 4 and 8 mildly abnormal; a score between 9 and 11 moderately abnormal; and a score >11 severely abnormal. To match the results with coronary angiograms, the 17 segments were grouped into the territories of the 3 main coronary arteries, as previously described:[19] left anterior descending artery (LAD), left circumflex artery (LCx) and right coronary artery (RCA). Thus, a regional SSS score could be calculated. Quantitative analysis was performed using MPI polar maps and the 17-segment model of the LV; uptake was normalized to 100% peak activity and the relative myocardial uptake (percent of maximum myocardial uptake) was assessed for each segment. In addition, LV volume and ejection fraction (EF) were measured after stress and at rest using previously validated software.[20]

Normal Database Group

Sex-specific normal perfusion files for supine and prone position acquisitions by CZT SPECT were derived from a group of 30 patients (15 female, 15 male) from the NIPPON DATA 80 study who had a low likelihood (LLk) of CAD (<5%) based on sex, age, systolic blood pressure (SBP), serum total cholesterol, serum glucose and smoking habit at the time of MPS.[21] Nine patients had normal coronary arteries. No patients in that group had diabetes mellitus, hypertension, hypercholesterolemia, or a smoking habit. Furthermore, all had normal stress and rest MPS images (segmental summed score <2).

CAG Analysis

Selective conventional CAG was performed using 5-Fr catheters. The angiograms were interpreted by 2 experienced cardiologists who were blinded to any other results. Identification of the coronary tree was based on a standard 15-coronary-segment model. Quantitative angiographic analysis was performed using the most severe, well-defined lesion in each segment via the digital caliper method. Significant stenosis was defined as a reduction in diameter ≥70%, except for the left main trunk, for which stenosis was defined as reduction ≥50%. If multiple abnormal segments were observed in an artery, the vessel was classified according to the status of the worst segment. Stenosis of the left main trunk was classified as double-vessel disease with stenosis in both the LAD and LCx.

Table 1. Clinical Subject Characteristics

Characteristic	All patients	CAG patients
No. patients	270	76
Male	171 (63)	46 (60.5)
Age (years)	69±11	71±9
BMI (kg/m²)	24.3±3.9	24.5±3.9
CV risk factors		
Smoking	124 (45.9)	36 (47.4)
Diabetes mellitus	112 (41.5)	25 (32.9)
Hypertension	187 (69.2)	51 (67.1)
Dyslipidemia	119 (44.1)	36 (47.4)
Positive family history	48 (17.8)	17 (22.4)
Clinical symptoms		
Typical angina pectoris	78 (28.9)	10 (13.2)
Atypical chest pain	42 (15.6)	11 (14.5)
Dyspnea	26 (9.6)	8 (10.5)
Previous cardiac events		
Previous MI	35 (13.0)	9 (11.8)
PCI	57 (21.1)	27 (35.6)

Data given as mean±SD or n (%).
BMI, body mass index; CAG, coronary angiography; CV, cardiovascular; MI, myocardial infarction; PCI, percutaneous coronary intervention.

Statistical Analysis

Continuous variables are presented as mean±SD. Where indicated, differences were assessed using Student's t-test for paired data and by 1-way repeated measures analysis of variance for 3 variables. Intra- and interobserver variability were measured using percent agreement and kappa values. Accuracy in the detection of coronary stenosis was assessed in terms of the area under the receiver operating characteristic (ROC) curve (AUC). The optimal cut-off points were determined to be those yielding minimal values for $(1\text{-sensitivity})^2+0.95\times(1\text{-specificity})^2$. $P<0.05$ was defined as indicative of statistical significance. The sensitivity and specificity of the different acquisition techniques were compared using paired McNemar test. Analysis was done using SPSS version 21 (SPSS, Chicago, IL, USA) and JMP 9 (SAS Institute, Cary, NC, USA).

Results

Patient Characteristics

Clinical characteristics of the entire patient group and of the patients who underwent CAG are given in **Table 1**. The mean age was 69±11 years and mean body mass index was 24.3±3.9 kg/m². Patients were referred for MPS for the following reasons: suspected CAD (n=136, 50.3%), follow-up of known CAD (n=116, 43.0%), and preoperative risk assessment before major noncardiac surgery (n=18, 6.7%). Seventy-eight (28.9%) of the present patients had typical angina, 42 patients (15.6%) had atypical angina and 26 (9.6%) had dyspnea. Previous myocardial infarction was present in 35 patients (13.0%), and 57 (21.1%) had undergone revascularization by means of coronary angioplasty.

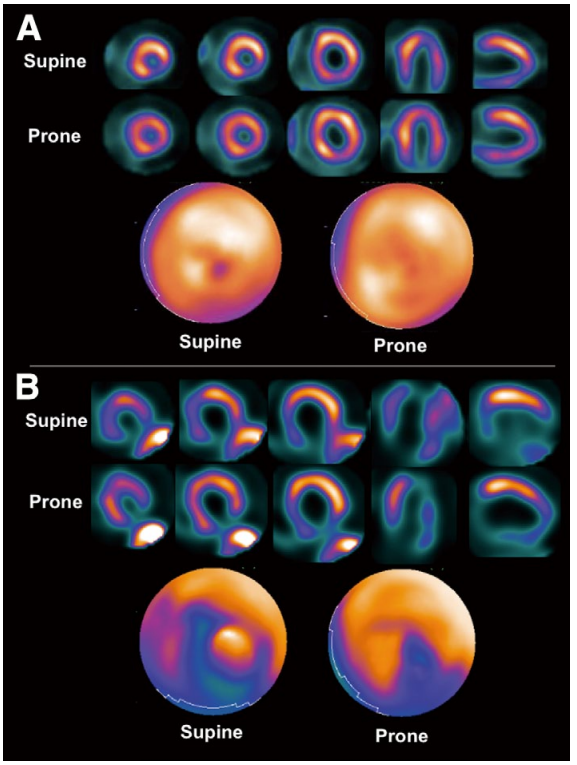

Figure 2. (**A**) Cadmium zinc telluride (CZT) single-photon emission computed tomography (SPECT) images from a 70-year-old man with typical chest pain. Post-stress images are displayed in a (**Top**) supine and (**Middle**) prone position in 3 short-axis views as well as in vertical and horizontal long-axis views and (**Bottom**) bull's eye maps. Reduced uptake of the radiotracer in the inferior wall is shown in the supine images, but no significant defect is visible in the prone images. Subsequent coronary angiogram indicated no significant stenosis. (**B**) CZT SPECT images from a 58-year-old man with chest pain on exertion whose subsequent coronary angiogram showed occlusions of the proximal right coronary artery and severe stenosis of the proximal left anterior descending artery. The supine tomography slices show subphrenic organ activity adjacent to the heart. (**Bottom**, **Left**) The subphrenic organ activity is back-projected onto the heart and is included in the polar map as myocardial activity. Imaging in the prone position, which moves the subphrenic organ further away from the heart, clearly shows the inferoposterior perfusion defect.

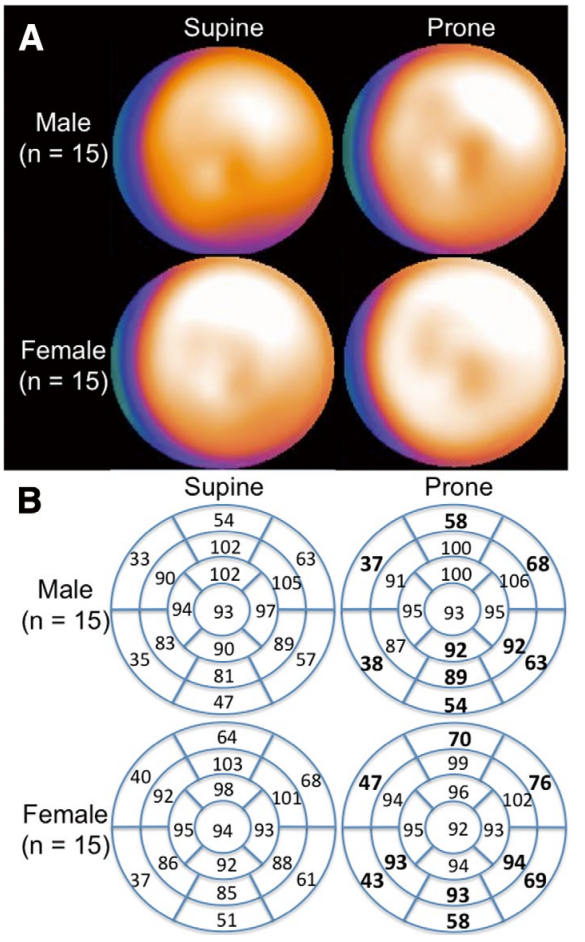

Figure 3. (**A**) Polar maps for stress ^{99m}Tc myocardial perfusion images derived from men (n=15) and women (n=15) with a low likelihood of coronary artery disease. (**Top**) Stress polar maps in men: (**Left**) supine and (**Right**) prone. (**Bottom**) Corresponding female polar maps. (**B**) Average myocardial uptake in the (**Left**) supine and (**Right**) prone positions among (**Top**) men and (**Bottom**) women. Bold, significant difference between the supine and prone images (P<0.05).

Hemodynamic Response to ATP

ATP is a precursor of adenosine and its hyperemic effect is thought to be equivalent to its degradation product, adenosine.[11,12] In all patients, ATP infusion caused some increase in heart rate and some decrease in SBP and diastolic BP (DBP). The baseline heart rate was significantly increased from 65.2±10.5 beats/min to 75.0±11.9 beats/min during ATP infusion (P<0.0001). Baseline SBP was significantly decreased from 159.4±22.5 mmHg to 143.2±23.8 mmHg (P<0.0001), and baseline DBP was significantly decreased from 76.5±10.7 mmHg to 69.4±12.6 mmHg (P<0.0001). All symptoms and hemodynamic changes were tolerated and disappeared within 1–2 min after discontinuation of ATP infusion. No severe adverse events were observed during pharmacological stress induction.

Image Quality

Stress supine images were graded as good or excellent in 263 of the 270 patients (97.4%), and stress prone images as good or excellent in 269 (99.6%; P=NS). Resting supine images were graded as good or excellent in 267 of the 270 patients (98.9%), and rest prone images as good or excellent in 269 (99.6%). The intra- and interobserver variability was 91% (kappa, 0.85; 95% confidence interval [CI]: 0.70–0.95%) and 85% (kappa, 0.76; 95% CI: 0.72–0.9), respectively. The mean grade for the stress prone images was significantly greater than that for the stress supine images (3.73±0.51 vs. 3.89±0.32, P<0.001). In addition, the mean grade for the rest prone images was significantly greater than that for the rest supine images (3.84±0.40 vs. 3.94±0.25, P<0.001). In 7 cases, supine images showed reduced uptake of the radiotracer in the inferior wall, while no significant defect was visible in the prone images (**Figure 2A**).

Only 2 patients in the entire prone examinations received an extra-cardiac activity grade of 3 (**Figure 2B**). In all, 21 patients (8%) received an extra-cardiac grade of 2 for the rest prone images compared with 56 (21%) for the rest supine images. Extra-cardiac activity was significantly less commonly observed in the stress prone vs. supine images (1.10±0.32 vs. 1.32±0.57,

Table 2. Coronary Angiography Findings (n=76)

Parameter	No. patients
Maximum stenosis ≥70%	54
Maximum stenosis <70%	22
Stenotic coronary arteries	
Single-vessel disease	26
Double-vessel disease	21
Triple-vessel disease	7
Left main	6
Left anterior descending	34
Left circumflex	32
Right coronary	23

P<0.001) as well as in the rest prone vs. supine images (1.05±0.23 vs. 1.20±0.45, P<0.001). Sex, weight, and the perfusion agents used had no significant effects on image quality (data not shown).

Mean Myocardial Perfusion

In Figure 3A, the average count distributions derived from 15 men and 15 women with an LLk of CAD are presented using a polar map display. In Figure 3B, mean count distributions are shown using a 17-segment model. The ranges of segmental average deviations in supine and prone men were 3.7–6.7% and 3.1–7.6% for LAD, 4.5–8.5% and 3.7–7.4% for LCX, and 4.5–8.5% and 3.3–9.3% for RCA, respectively. Those in women were 4.0–10.2% and 4.4–12.1% for LAD, 5.7–10.9% and 5.0–11.6% for LCX, and 5.0–10.0% and 4.3–12.3% for RCA, respectively. The average myocardial uptake differed significantly between the supine and prone positions in 9 of the 17 segments in both men and women (P<0.05). Segmental differences between the supine and prone images were noted predominantly in the inferior and proximal distributions in both male and female subjects (Figure 3).

Coronary Anatomy

Of the 76 patients who underwent CAG, 22 (29%) had normal coronary arteries (Table 2) and 26 (34%), 21 (28%) and 7 (9%) had 1-, 2- and 3-vessel disease, respectively. Regarding the distribution of significant stenoses, we observed 6, 34, 32, and 23 left main, LAD, LCx, and RCA lesions, respectively.

Image Interpretation and Correlation With CAG

Stress supine images were graded as "normal", "mildly abnormal", "moderately abnormal" and "severely abnormal" in 21, 31, 9, and 15 of the 76 patients. The intra- and interobserver variability was 89% (kappa, 0.85; 95% CI: 0.75–0.95%) and 80% (kappa, 0.72; 95% CI: 0.68–0.84), respectively.

The SSS for the supine (S-SSS), prone (P-SSS) and combined supine and prone (C-SSS) positions was 9±8 (range, 0–34), 7±8 (range, 0–29), and 7±8 (range, 0–29), respectively (P<0.0001). The SRS for the supine, prone, and combined supine and prone positions was 5±8 (range, 0–29), 4±7 (range, 0–27), and 6±7 (range, 0–24), respectively (P=0.005). The ROC curves for the detection of CAD by SSS measures derived from supine and prone vs. combined supine and prone datasets are shown in Figure 4. The AUC for the S-SSS, P-SSS, and C-SSS were 0.815 (95% CI: 0.713–0.917); 0.813 (95% CI: 0.711–0.914); and 0.872 (95% CI: 0.783–0.961), respectively. Thus, the AUC for C-SSS was greater than that for S-SSS or P-SSS (χ^2=1.60, P=0.21; or χ^2=1.32, P=0.25, respectively).

As shown in Figure 5, using an SSS cut-off value of >3.5,

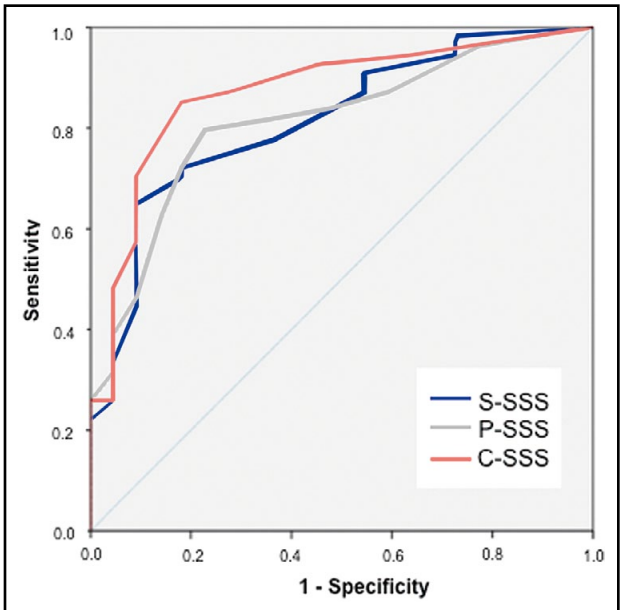

Figure 4. Receiver operating characteristic curves for the detection of coronary artery disease on summed stress scores (SSS) for the supine (S-SSS), prone (P-SSS) and combined supine and prone (C-SSS) positions in the angiography group (n=76).

the sensitivities for the detection of CAD of the S-SSS, P-SSS, and C-SSS were 78%, 80%, and 85%, respectively (P=NS). The corresponding specificities were 50%, 77%, and 82%. The accuracy of S-SSS, P-SSS, and C-SSS was 76%, 78%, and 85%, respectively. The specificity of C-SSS was significantly better than that of S-SSS (P=0.021). Consequently, the accuracy of C-SSS was also significantly better than that of S-SSS (P=0.035).

Per-Vessel Analysis

On a per-vessel basis, using SSS ≥2 for the detection of significant stenosis, the sensitivity and specificity of the supine images were 70% and 63% compared with 72% and 71% for the prone images, and 65% and 71% for the combined supine and prone images. The sensitivity was relatively unchanged among S-SSS, P-SSS, and C-SSS (not significant), but the specificity was significantly different between S-SSS and C-SSS (P=0.027). The sensitivity and specificity of the combined supine and prone images were 52.9% and 81.0% for LAD, 71.9% and 65.9% for LCX, and 73.9% and 67.9% for RCA, respectively.

LV Volumes and EF

In the resting examination, the end-diastolic volume was 91.2±33.2 ml during supine imaging, which was significantly larger than the 86.3±32.7 ml observed during prone imaging (P=0.001). The end-systolic volumes were 39.0±29.1 ml and 37.6±28.5 ml, respectively (P=NS). EF was 62.7±12.8% during supine imaging, which was greater than the 61.3±14.0% observed during prone imaging.

In the stress examination, the end-diastolic volume was 92.8±33.1 ml during supine imaging, which was significantly larger than the 89.1±32.9 ml observed during prone imaging (P=0.034). The end-systolic volume was 43.1±31.0 ml vs. 40.3±29.3 ml (P=NS), and the EF 59.6±13.5% vs. 59.1±13.5%, respectively (P=NS).

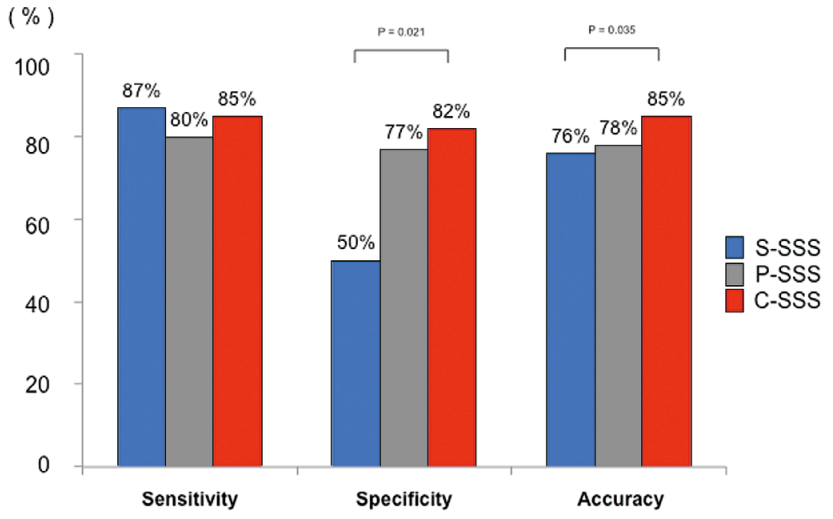

Figure 5. Sensitivities, specificities and accuracies of coronary artery disease detection in the angiography group (n=76). C-SSS, summed stress score for the combined prone and supine positions; P-SSS, summed stress score for the prone position; S-SSS, summed stress score for the supine position.

Discussion

To the best of our knowledge, this is the first study to use the novel CZT camera in conjunction with combined supine and prone imaging for the detection of hemodynamically significant CAD and to compare its diagnostic accuracy with that of CAG. We confirmed the good image quality of both supine and prone CZT SPECT and noted that the sensitivity, specificity, and accuracy for the detection of CAD were 85%, 82%, and 85%, respectively, with the combined supine and prone approach. In 7 out of 76 patients (9.2%), reduced uptake of the radiotracer by the inferior wall was seen in the supine images, but no significant defect was visible in the prone images. This was the major reason for the combined supine and prone imaging having significantly better specificity than supine or prone imaging alone. For individual coronary territories, we noted a sensitivity and specificity of 65% and 71%, respectively. The results are similar to those found in previous studies that have used the conventional Anger camera.[22]

Recently, using another type of CZT gamma camera, the D-SPECT (Spectrum Dynamics, Caesarea, Israel), Nakazato et al introduced a combined upright and supine imaging protocol and reported that this protocol has good diagnostic accuracy for detecting CAD.[23] Prone imaging is not possible with the D-SPECT system and there may be some difference between prone and upright acquisition. They also stated that the exact mechanism by which the test performance was improved by combining the supine and upright positions was not clear and warranted further investigation.[24]

Feasibility of Combined Image Acquisition Using CZT Camera

Combined supine and prone MPS using conventional Anger cameras is time-consuming, because it requires at least 30–40 min. Therefore, the approach is not widely used.[24] Compared with conventional Anger cameras, combined acquisition using the novel CZT cameras may be more practical because the imaging times are much shorter. In the present protocol using the Discovery NM530c, the mean time required for repositioning a patient is 3±2 min. Accordingly, the total acquisition time of combined supine and prone imaging was a maximum of 15 min, which may be acceptable for almost all patients. In fact, 270 of the 276 patients (97.8%) in the present series completed the combined acquisition protocol without any serious complaint.

Another concern about prone imaging with conventional Anger cameras is that it results in slightly lower total myocardial photon count compared with supine imaging, most likely due to the increase in the camera-to-chest wall distance. Kiat et al reported that the mean distance is 16.3±2.9 cm for prone imaging compared with 13.5±4.1 cm for supine imaging with the conventional Anger camera.[4] We found that with the Discovery NM530c the distance was 2.5±0.6 cm for the supine position and 7.1±1.2 cm for the prone position. In addition, we found that the end-diastolic volume as well as the LVEF was significantly larger during supine compared with prone imaging via a wall motion assessment from gated CZT SPECT. This may be due to the close distance between the anterior chest wall and the imaging table in the prone position. A possible drawback is the fact that prone images are acquired through the imaging table (1.5 cm in width), which may elicit attenuation and scattered radiations and impair image quality. Nevertheless, image quality analysis confirmed that the quality of prone images was similar to that of supine images.

Advantages of Combined Image Acquisition

We found that extra-cardiac activity was significantly less frequently observed in CZT SPECT images acquired in the prone position compared with the supine position. Consequently, the overall quality of prone imaging was significantly greater than that of supine imaging. We also derived normal perfusion polar maps for CZT SPECT in both the supine and prone positions from 15 men and 15 women with an LLk of CAD. The average myocardial uptake differed significantly between the supine and prone CZT SPECT and the differences were noted predominantly in the inferior and proximal distributions in both male and female subjects.

In previous studies performed using conventional Anger cameras, the prone position has been shown to reduce diaphragmatic attenuation.[1–6] The reduction in attenuation is considered to be due to a downward displacement of the diaphragm and subphrenic organs, such as the liver or intestine, and an upward displacement of the heart, which increases the distance between the inferior wall of the LV and diaphragm in the prone position.[2,5] The present CZT SPECT observations are consistent

with these previous findings.

Prone acquisition, however, has been reported to produce artifactual anteroseptal defects, which are thought to be due to the closer position of the heart to the bony structures of the anterior chest wall.[4] We also found artifactual anterior defects in 5 of the 76 patients (6.6%) who underwent CAG. We therefore developed a combined defect score that was calculated by grouping the anterior defects observed during supine imaging with inferior half segments observed during prone imaging. Using the combined defect score, artifactual anterior defects on the prone images and inferoposterior to lateral defects on the supine images can be attenuated. Consequently, the AUC of combined supine and prone imaging was greater than that for supine or prone imaging alone. Finally, combined supine and prone CZT SPECT yielded significant gains in specificity and accuracy compared with supine imaging alone despite the absence of any attenuation correction.

Study Limitations

The study was limited by the fact that the assessments were performed at a single site. The study group consisted of consecutive patients referred by physicians, and only a subgroup underwent CAG. The use of stress MPS as a clinical gatekeeper for catheterization means that most patients referred for CAG have abnormal myocardial perfusion. This referral bias results in a selection bias and may result in a lower sensitivity and specificity for supine imaging, but it does reflect the actual clinical situation.

All images were analyzed visually using 4-mm-thick short axis slices other than polar maps to obtain the SSS and SRS scores. Given that the database was created from data from a relatively small number of patients, we could not use automatic calculation software for the combined supine and prone images. We intend to calculate scores automatically in a future project.

Conclusions

Combined supine and prone SPECT acquisition with a novel CZT camera is a practical means of reducing the false-positive rate associated with supine image acquisition, and has high diagnostic accuracy for detecting clinically significant CAD compared with CAG. This is a simple modification that is easy to perform and acceptable to almost all patients. Moreover, it does not lengthen the time of image acquisition or increase radiation exposure.

Acknowledgments

The authors declare no conflicts of interest.

References

1. Segall GM, Davis MJ, Goris ML. Improved specificity of prone versus supine thallium SPECT imaging. *Clin Nucl Med* 1988; **13:** 915–991.
2. Segall GM, Davis MJ. Prone versus supine thallium myocardial SPECT: A method to decrease artifactual inferior wall defects. *J Nucl Med* 1989; **30:** 548–555.
3. Esquerre JP, Coca FJ, Martinez SJ, Guiraud RF. Prone decubitus: A solution to inferior wall attenuation in thallium-201 myocardial tomography. *J Nucl Med* 1989; **30:** 398–401.
4. Kiat H, Van Train KF, Friedman JD, Germano G, Silagan G, Wang FP, et al. Quantitative stress-redistribution thallium-201 SPECT using prone imaging: Methodologic development and validation. *J Nucl Med* 1992; **33:** 1509–1515.
5. DePuey EG. How to detect and avoid myocardial perfusion SPECT artifacts. *J Nucl Med* 1994; **35:** 699–702.
6. Nishina H, Slomka PJ, Abidov A, Yoda S, Akincioglu C, Kang X, et al. Combined supine and prone quantitative myocardial perfusion SPECT: Method development and clinical validation in patients with no known coronary artery disease. *J Nucl Med* 2006; **47:** 51–58.
7. Bocher M, Blevis IM, Tsukerman L, Shrem Y, Kovalski G, Volokh L. A fast cardiac gamma camera with dynamic SPECT capabilities: Design, system validation and future potential. *Eur J Nucl Med Mol Imaging* 2010; **37:** 1887–1902.
8. Herzog BA, Buechel RR, Katz R, Brueckner M, Husmann L, Burger IA, et al. Nuclear myocardial perfusion imaging with a cadmium-zinc-telluride detector technique: Optimized protocol for scan time reduction. *J Nucl Med* 2010; **51:** 46–51.
9. Buechel RR, Herzog BA, Husmann L, Burger IA, Pazhenkottil AP, Treyer V, et al. Ultrafast nuclear myocardial perfusion imaging on a new gamma camera with semiconductor detector technique: First clinical validation. *Eur J Nucl Med Mol Imaging* 2010; **37:** 773–778.
10. Sharir T, Slomka PJ, Hayes SW, DiCarli MF, Ziffer JA, Martin WH, et al. Multicenter trial of high-speed versus conventional single-photon emission computed tomography imaging: Quantitative results of myocardial perfusion and left ventricular function. *J Am Coll Cardiol* 2010; **55:** 1965–1974.
11. Gimelli A, Bottai M, Giorgetti A, Genovesi D, Kusch A, Ripoli A, et al. Comparison between ultrafast and standard single-photon emission CT in patients with coronary artery disease: A pilot study. *Circ Cardiovasc Imaging* 2011; **4:** 51–58.
12. Tanaka H, Chikamori T, Hida S, Uchida K, Igarashi Y, Yokoyama T, et al. Comparison of myocardial perfusion imaging between the new high-speed gamma camera and the standard anger camera. *Circ J* 2013; **77:** 1009–1017.
13. Esteves FP, Raggi P, Folks RD, Keidar Z, Askew JW, Rispler S, et al. Novel solid-state-detector dedicated cardiac camera for fast myocardial perfusion imaging: Multicenter comparison with standard dual detector cameras. *J Nucl Cardiol* 2009; **16:** 927–934.
14. Coma-Canella I, Palazuelos J, Bravo N, Velloso MJG. Myocardial perfusion imaging with adenosine triphosphate predicts the rate of cardiovascular events. *J Nucl Cardiol* 2006; **13:** 316–323.
15. Yoshinaga K, Tomiyama Y, Suzuki S, Tamaki N. Myocardial blood flow quantification using positron-emission tomography: Analysis and practice in the clinical setting. *Circ J* 2013; **77:** 1662–1671.
16. Berman DS, Kang X, Tamarappoo B, Wolak A, Hayes SW, Nakazato R, et al. Stress thallium-201/rest technetium-99m sequential dual isotope high-speed myocardial perfusion imaging. *JACC Cardiovasc Imaging* 2009; **2:** 273–282.
17. ICRP Publication 80: Radiation dose to patients from radiopharmaceuticals (Addendum 2 to ICRP publication 53). *Ann ICRP* 1998; **28:** 1–126.
18. ICRP Publication 106: Radiation dose to patients from radiopharmaceuticals (Addendum 3 to ICRP publication 53). *Ann ICRP* 2008; **38:** 1–197.
19. Cerqueira MD, Weissman NJ, Dilsizian V, Jacobs AK, Kaul S, Laskey WK, et al. Standardized myocardial segmentation and nomenclature for tomographic imaging of the heart: A statement for healthcare professionals from the cardiac imaging committee of the council on clinical cardiology of the American Heart Association. *Circulation* 2002; **105:** 539–542.
20. Germano G, Kiat H, Kavanagh PB, Moniel M, Mazzanti M, Su HT, et al. Automatic quantification of ejection fraction from gated myocardial perfusion SPECT. *J Nucl Med* 1995; **36:** 2138–2147.
21. Ueshima H, Kasagi F, Kodama K, Okamura T, Hayakawa T, Okayama A, et al. (NIPPON DATA 80 Research Group). Risk assessment chart for death from cardiovascular disease based on a 19-year follow-up study of a Japanese representative population: NIPPON DATA80. *Circ J* 2006; **70:** 1249–1255.
22. Klocke FJ, Baird MG, Lorell BH, Bateman TM, Messer JV, Berman DS, et al. American College of Cardiology; American Heart Association Task Force on Practice Guidelines; American Society for Nuclear Cardiology. ACC/AHA/ASNC guidelines for the clinical use of cardiac radionuclide imaging: Executive summary: A report of the American College of Cardiology/American Heart Association Task Force on practice guidelines (ACC/AHA/ASNC Committee to Revise the 1995 Guidelines for the Clinical Use of Cardiac Radionuclide Imaging). *Circulation* 2003; **108:** 1404–1418.
23. Nakazato R, Tamarappoo BK, Kang X, Wolak A, Kite F, Hayes SW, et al. Quantitative upright-supine high-speed SPECT myocardial perfusion imaging for detection of coronary artery disease: Correlation with invasive coronary angiography. *J Nucl Med* 2010; **51:** 1724–1731.
24. Hayes SW, De Lorenzo A, Hachamovitch R, Dhar SC, Hsu P, Cohen I, et al. Prognostic implications of combined prone and supine acquisitions in patients with equivocal or abnormal supine myocardial perfusion SPECT. *J Nucl Med* 2003; **44:** 1633–1640.